Nanoscale

Accepted Manuscript

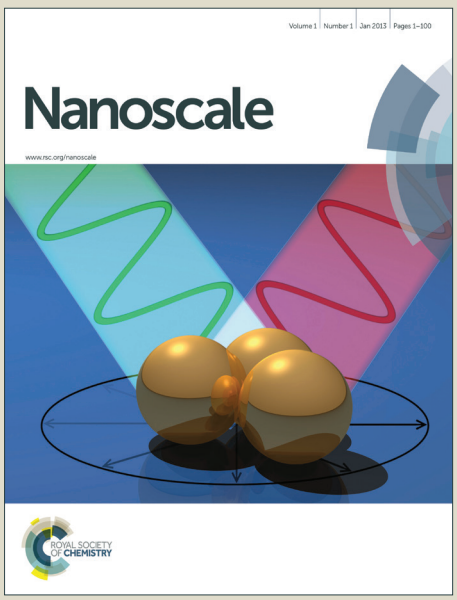

ROYAL SOCIETY OF CHEMISTRY

www.rsc.org/nanoscale

ARTICLE TYPE www. rsc.org/xxxxxx | XXXXXXXX

AC Conductivity Parameters of Graphene Derived from THz Etalon Transmittance†

Weidong Zhang,*[a] Phi Huy Quoc Pham,[b] Elliott R. Brown,[a] and Peter Burke,[b]

Received Xth XXXXXXXXXX 20XX, Accepted Xth XXXXXXXXX 20XX
First published on the web Xth XXXXXXXXXX 200X
DOI: 10.1039/b000000x

THz frequency-domain transmittance measurements are carried out on chemical-vapor-deposition (CVD) graphene films transferred to high-resistivity silicon substrates, and packaged as a back-gated graphene field effect transistor (G-FETs). The graphene AC conductivity $\sigma(\omega)$, both real and imaginary parts, is determined between 0.2 and 1.2 THz from the transmittance using the transmission matrix method and curve-fitting techniques. Critical parameters such as charge-impurity scattering width and chemical potential are calculated. It is found that not only the sheet charge density but also the scattering parameter can be modified by the back-gate voltage.

1 Introduction

For monolayer graphene-based devices such as the high speed field effect transistor (FET), electronically gated optical modulator and two dimensional plasmonic devices, the ac conductivity $\sigma(\omega)$ is an important parameter which has been studied both theoretically and experimentally.[1–7] In this letter, we demonstrate a terahertz (THz) etalon transmittance technique in the frequency domain and apply it to obtain the graphene complex conductivity in the range 0.2-1.2 THz. Previously, conductivity in this frequency range was usually extrapolated from either RF or infrared data, or obtained at spot frequencies.[8] There was also a report on measurements with time domain THz spectroscopy, but no frequency dependence $\sigma(\omega)$ was provided.[9] The approach reported here derives the conductivity directly from the THz transmittance data and is non-contact and non-destructive. Compared with dc methods, the THz can provide "quieter" measurements with less presence of noise (e.g. 1/f noise). Compared with visible-wavelength methods, the THz provides low propagation loss through the graphene-bearing silicon substrates. Compared with IR methods, the THz photon energy ($\sim$ 4.0 meV at 1 THz) mostly induces intraband transitions, and is less likely to excite interband transitions (Fig. 1).

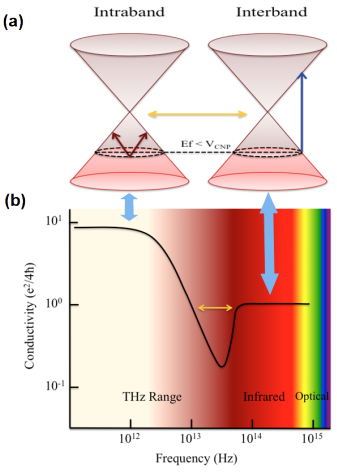

Fig. 1 Qualitative illustration of the spectral transitions in graphene that contribute to the AC conductivity.

2 THz Etalon Transmittance Measurements

To prepare the graphene for THz testing, first a 1 cm x 1 cm monolayer graphene film was grown on copper foil using CVD. Next poly-methyl methacrylate (PMMA) was spun onto the graphene film. The copper foil was then etched away overnight in ammonium persulfate. The floating graphene was cleaned in DI water, and wet transferred onto the 90-nm-thick SiO_2 layer pre-deposited on a high-resistivity silicon substrate. Then the PMMA was removed with acetone wash, and annealed in a hydrogen+argon atmosphere. The quality of the transferred graphene film was confirmed using Raman spectroscopy; the two characteristic G and 2D peaks at $\sim$1591 cm^{-1}, and $\sim$2683 cm^{-1}, respectively, were clearly observed

† Electronic Supplementary Information (ESI) available: [details of any supplementary information available should be included here]. See DOI: 10.1039/b000000x/

[a] *Terahertz Sensors Laboratory, Depts. of Physics and Electrical Engineering, Wright State University, Dayton, OH, USA, 45435. E-mail: weidong.zhang@wright.edu*
[b] *Dept. of Electrical Engineering and Computer Science, University of California, Irvine, CA, USA, 92697.*

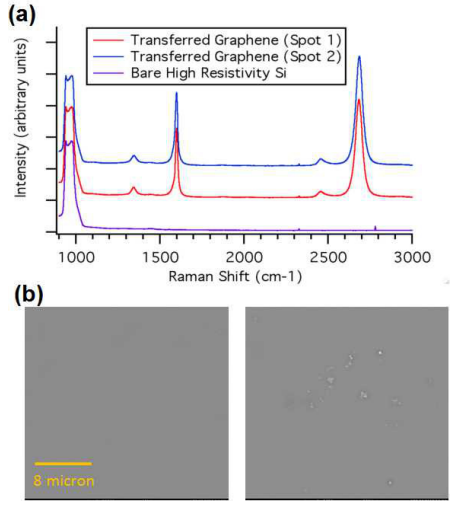

Fig. 2 (a) The Raman spectrum before and after graphene transfer to silicon. (b) The SEM images of graphene film transferred to silicon after annealing process.

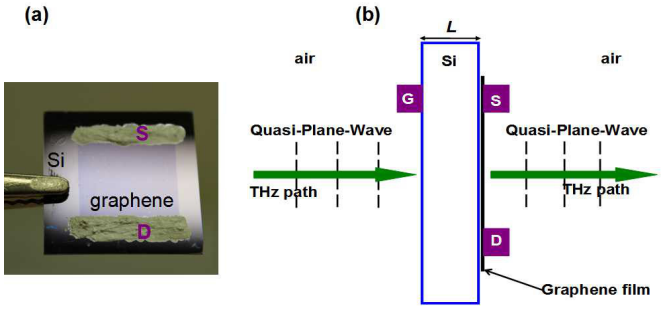

Fig. 3 (a) The G-FET, and (b) the THz Fabry Perot Etalon setup. S: source; D: drain; G: back gate.

indicating monolayer graphene coverage [Fig. 2 (a)]. Two smaller but visible peaks at $\sim$1350 cm^{-1} and $\sim$2445 cm^{-1} are related to defect-induced Raman scattering.[10] Scanning electron microscope (SEM) inspection showed the large-area graphene film to be mostly clean after the annealing process [the left of Fig. 2 (b)]. However, small speckles of residual PMMA are observed [the right of Fig. 2 (b)].

To package a back-gated G-FET, two electrodes - the source and drain - were deposited with silver paint on two opposite ends of the graphene film; a third terminal the gate was deposited on the back side of the silicon [Fig. 3].

Figure 4 shows the dc characteristics of the G-FET, source-drain I-V curve in (a), and the C-V curve in (b). From the slope of Fig. 4 (a) at zero gate voltage, we obtain a dc sheet conductance of 19.7 $e^2/4\hbar$, where $e^2/4\hbar$ is the accepted optical (interband) conductance of monolayer graphene.[4] Our dc conductance exceeds the optical because of the stronger ef-

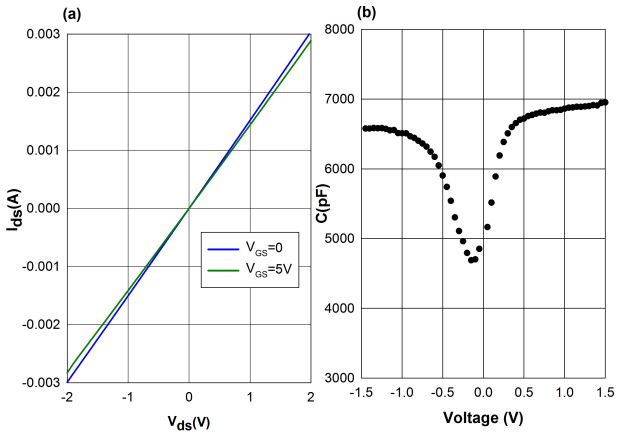

Fig. 4 The source-drain current vs. voltage (I_{DS}-V_{DS}) curves at different gate voltages (V_{GS}). (b) The C-V curve measured at 30 Hz with ac amplitude 100 mV.

fect of intraband compared to interband transport. The G-FET shows but modest transconductance - a value of 0.68 mS occurring at V_{DS}=2 V and V_{GS}=0 V. This is because of the large separation from the graphene to the back gate, whereby most of the applied gate voltage drops across the silicon and oxide layers. The C-V curve in Fig. 4 (b) supports this interpretation, displaying a dip in capacitance just below zero bias as expected from metal-insulator-semiconductor theory with a back-gate and n-type substrate. At a larger negative gate bias, the silicon goes into inversion, and at positive bias, it goes into accumulation. This is consistent with the known n-type nature of our high-resistivity Si, having a doping concentration of $\sim 10^{14}/\mathrm{cm}^3$.

To measure the THz transmittance, an Emcore PB7100 frequency-domain transceiver was used. It sweeps continuously from 0.1 to 1.6 THz in steps of 500 MHz with a dynamic range of approximately 80 dB at 0.1 and 40 dB at 1.0 THz. The diameter of THz beam is $\sim$3 mm. First a background scan without any sample in the THz beam path was performed, and the scan was recorded as $P_{\mathrm{B}}(f)$. Next the noise floor scan was acquired by blocking the beam with a metallic plate, and the signal was recorded as $P_{\mathrm{N}}(f)$. Then the G-FET sample was placed in the beam path, and the scan was recorded as $P_{\mathrm{S}}(f)$. Finally, the transmittance was calculated from $T_e = [P_{\mathrm{S}}(f) - P_{\mathrm{N}}(f)]/[P_{\mathrm{B}}(f) - P_{\mathrm{N}}(f)]$.

A bare oxide-on-Si substrate (control sample) having the same physical properties as the G-FET substrate was measured in room temperature (T=300K). The substrate was almost lossless, as demonstrated by the multiple interference peaks in the transmittance having their maxima close to 1.0 [Fig. 5 (a)]. This is also characteristic of a balanced etalon where the two interface (air-Si and Si-air) reflectivities are equal. Then the G-FET sample was measured. Its transmit-

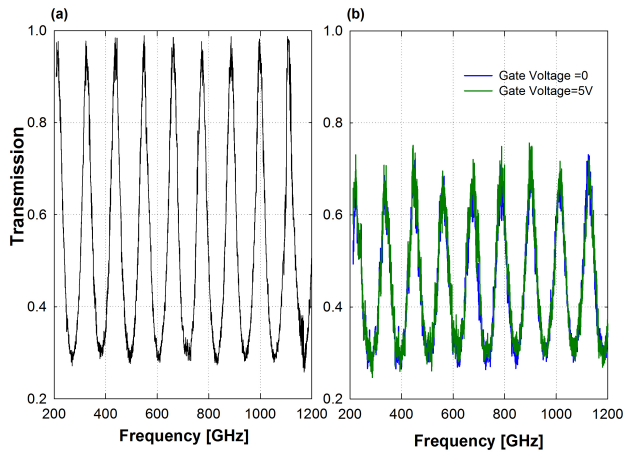

Fig. 5 (a) The transmission of bare Si as a control sample. (b) The transmission of graphene film on Si substrate.

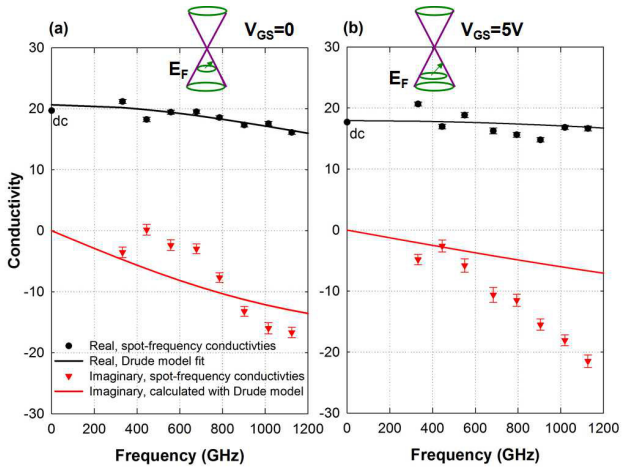

Fig. 6 (a) The fitting of the conductivities at V_{GS}=0. The unit of conductivity is $e^2/4\hbar$. (b) The fitting of conductivities at V_{GS}=5V. The discrete data points are spot-frequency conductivities from fit to the transmittance peaks, circles being real part and inverted triangles imaginary. The continuous line of real is the Drude-model fit to the spot-frequency real conductivity points, and the continuous line of imaginary is calculated with the Drude-model using the extracted Γ and μ.

tance spectrum is plotted in Fig. 5 (b) for two gate bias voltages of 0 and 5.0 V. In both cases there are multiple peaks and valleys due to the interference effect in the G-FET etalon, but the maxima are reduced considerably below those in Fig. 5 (b) because of imbalance in the reflectivity at the two interfaces. When the back-gate voltage was set to 5.0 V, a modest change occur in the transmittance at some of the peaks but there was insignificant change at the valleys between the peaks.

3 Modeling and Discussion

The THz conductivity of the graphene is determined using the transmission matrix method (TMM).[11] The THz beam was incident normally. Its transmittance is $T_e = |S_{21}|^2$ with

$$S_{21} = \frac{t_1 t_2 \exp(-jk_s L)}{1 + r_1 r_2 \exp(-2k_s L)} \tag{1}$$

where L is the thickness of the Si substrate, k_s is the wave vector inside the substrate. k_s is equal to $2\pi\sqrt{\varepsilon_s}/\lambda$, where ε_s is the dielectric constant of silicon and λ is the free-space wavelength. r_1 and t_1 are the coefficients of reflection and transmission at the front air/Si interface, respectively, and are given by

$$r_1 = \frac{1-\sqrt{\varepsilon_s}}{1+\sqrt{\varepsilon_s}} \tag{2}$$

$$t_1 = \frac{2}{1+\sqrt{\varepsilon_s}} \tag{3}$$

r_2 and t_2 are the coefficients of reflection and transmission at the Si/graphene/graphene/air interfaces, respectively,[1] and are given by

$$r_2 = \frac{\sqrt{\varepsilon_s} - (\sqrt{\varepsilon_g}+1)}{\sqrt{\varepsilon_s} + (\sqrt{\varepsilon_g}+1)} \tag{4}$$

$$t_2 = \frac{2\sqrt{\varepsilon_s}}{\sqrt{\varepsilon_s} + (\sqrt{\varepsilon_g}+1)} \tag{5}$$

where $\varepsilon_g = \mathtt{Re}\{\varepsilon_g\} + j\mathtt{Im}\{\varepsilon_g\}$ is the complex dielectric constant of graphene. Finally the complex sheet conductance is computed from ε_g as

$$\sigma_g = \frac{\sqrt{\varepsilon_g}}{Z_0} \tag{6}$$

where $Z_0 = 377\Omega$ is the impedance of free space.

The thickness of silicon substrate was L=392 μm. The value of silicon ε_s=11.65, is accurately known in the THz region and has insignificant frequency dependence.[12] To determine ε_g, and therefore σ_g, a least-squares fitting procedure is performed around each transmittance peak in Fig. 5 (b) using Equations (1-6) with $\mathtt{Re}\{\varepsilon_g\}$ and $\mathtt{Im}\{\varepsilon_g\}$ as fitting parameters.* Each fitting region includes a center frequency where a peak is located, and two end frequencies where the adjacent valleys are located. The real and imaginary parts of the THz conductivity at these center frequencies, are shown in Fig. 6 for unbiased (V_{GS}=0.0 V) and biased (V_{GS}=5.0 V)

*The scipy.optimize library of Python was used for the least-squares fitting , and its documentation can be found in www.SciPy.org. The curve_fit() is designed to minimize the sum of square of (f(xdata)-ydata), which is denoted as χ^2. We use reduced chi square $\tilde{\chi}^2$ to evaluate the goodness of the fittings. A fitting is regarded as good when $\tilde{\chi}^2$ is less than 1. $\tilde{\chi}^2$ is estimated from $\chi^2/(N-p)$, where N is the number of data points, and $p=2$ is the number of parameters for fitting. In the fitting of every transmittance peak region, $N \sim 110$, and $\tilde{\chi}^2$ is less than 0.1.

conditions. The error bars,including the system errors determined from the bare silicon measurement, are plotted too. The real conductivities have standard deviation of 2-3%; however, the imaginary conductivities have standard deviation as much as 50%. The real part of the conductivities ($\sim 20e^2/4\hbar$) are within the range of values extrapolated from FTIR data.[13] The broadband gate-bias dependence of the real and imaginary parts, especially between 400 and 900 GHz, is observed. Above 1.2 THz isn't plotted because the quality of the data is degrading. This is attributable to a decreasing dynamic range of the instrument and also multiple water-vapor lines that are not perfectly cancelled out by the normalization procedure.

Next the extracted THz conductivity, both real part and imaginary part, are compared to the theoretical model of intraband conductivity, which is commonly written as a Drudian form,[14,15]

$$\mathrm{Re}\{\sigma_{\mathrm{intra}}(\omega)\} = \frac{e^2}{4\hbar}\frac{2}{\pi}\frac{8k_BT\Gamma}{\hbar^2\omega^2+4\Gamma^2}\log\left[2\cosh\left(\frac{\mu}{2k_BT}\right)\right] \quad (7)$$

$$\mathrm{Im}\{\sigma_{\mathrm{intra}}(\omega)\} = -\frac{e^2}{4\hbar}\frac{2}{\pi}\frac{4k_BT\hbar\omega}{\hbar^2\omega^2+4\Gamma^2}\log\left[2\cosh\left(\frac{\mu}{2k_BT}\right)\right] \quad (8)$$

where k_B is the Boltzmann constant, e is the electron charge, $\hbar$ is the Planck constant, $\omega = 2\pi f$ is the angular frequency, Γ is a phenomenological parameter representing the magnitude of scattering, and μ is the chemical potential.

The two critical parameters Γ and μ are found by a least-squares fit to the real part of the conductivity only. The obvious deviation from the Drudian line at V_{GS}=5 V ($\sim 3\ e^2/4\hbar$) may be due to the dielectric response of PMMA residue and the inhomogeneity of the graphene film caused by PMMA [Fig. 2 (b)]. The fitting leads to the values Γ=4.60 meV, μ=-0.15 eV at V_{GS}=0 and Γ=9.23 meV, μ=-0.26 eV at V_{GS}=5 V, respectively. Accordingly, the scattering time constants $\tau = \hbar/2\Gamma$ are 72 fs at V_{GS}=0, and 36 fs at V_{GS}=5 V. Calculation with Eq. (7) then leads to a good agreement with the experimental values, as shown in Fig. 6. The dc values according to Eq.(7) are 20.63 and 17.94 $e^2/4\hbar$, respectively, which are very close to the ones measured directly from Fig. 4 (a). The relative differences are 4.7% at V_{GS}=0 and 1.4% at V_{GS}=5 V. This proves the accuracy of Eq. (7) as well as the consistency of experimental data from dc to THz.

The imaginary conductivity is calculated with Eq. (8) and the extracted Γ and μ are plotted in Fig. 6. The data points deviate from the Drudian lines by more than one error bar, but display the same trend globally as the Drude formula predicts. The possible reasons of deviation include the uncertainties of Si thickness and Si dielectric constant, which can sensitively shift the phasor of $\exp(-2k_sL)$ in Eq. (1). Other possible influence factors are the PMMA residue and the free carriers on the Si side of the Si-oxide interface.

Another possible consideration is the quantum capacitance of graphene defined as the variation of sheet charge density versus the change of chemical potential ($C_g \propto dn/d\mu$).[16] The chemical potential is controlled by the component of electric field perpendicular to the gate and graphene film, as is the charge density. However, the THz electric field is parallel to the graphene film. So it should not change μ or n, and therefore not be affected by the quantum capacitance.

The interband conductivity isn't included in the fitting procedure above either, because it is less significant compared to the intraband one given that the THz photon energy is much less than the chemical potential ($\hbar\omega \ll 2\mu$). This is verified with the following model[1]

$$\mathrm{Re}\{\sigma_{\mathrm{inter}}(\omega)\} \approx \frac{e^2}{4\hbar}\left\{\frac{1}{2}+\frac{1}{\pi}\arctan\left(\frac{\hbar\omega-2\mu}{2k_bT}\right)\right\} \quad (9)$$

$$\mathrm{Im}\{\sigma_{\mathrm{inter}}(\omega)\} \approx \frac{e^2}{4\hbar}\left\{-\frac{1}{2\pi}\log\left[\frac{(\hbar\omega+2\mu)^2+(2k_BT)^2}{(\hbar\omega-2\mu)^2+(2k_BT)^2}\right]\right\} \quad (10)$$

The real part is $\mathrm{Re}\{\sigma_{\mathrm{inter}}\} \sim 0.95\ e^2/4\hbar$ at μ=-0.15 eV (V_{GS}=0) and $0.97e^2/4\hbar$ at μ=-0.26 eV (V_{GS}=5 V), respectively. The imaginary part $\mathrm{Im}\{\sigma_{\mathrm{inter}}\}$ is -0.0083 $e^2/4\hbar$ at 1 THz.

4 Conclusions

In summary, the broadband THz conductivity of a monolayer graphene film is derived by a curve fitting procedure to the individual peaks of the etalon transmittance. The scattering parameter as well as the chemical potential - the two quantities critical to the intraband conductivity - are extracted. Both are modified by back-gate voltage. We note the extracted imaginary conductivity is less reliable because of its poor sensitivity factor †. For example, the sensitivity factor, defined as $S_I = \partial\log(T_e)/\partial\log(\mathrm{Im}\{\sigma_g\})$, is S_I=0.0013 at 338GHz; in contrast, the analogous sensitivity quantity for the real conductivity, defined as $\partial\log(T_e)/\partial\log(\mathrm{Re}\{\sigma_g\})$, is 0.4 at the same frequency. To obtain more precise imaginary conductivity, we are considering the combination of the above technique with frequency-domain reflectivity measurements.

References

1 L. A. Falkovsky and S. S. Pershoguba, *Physical Review B*, 2007, **76**, 153410 1–4.
2 T. Ando, *Journal of the physics society of Japan*, 2006, **75**, 074716 1–7.
3 M. R. V. Ryzhii and T. Otsuji, *Journal of Applied Physics*, 2007, **101**, 083114 1–4.
4 F. C. A. B. Kuzmenko, E. van Heumen and D. van der Marel, *Physics Review Letters*, 2008, **127**, 117401 1–4.
5 D. B. Farmer, V. Perebeinos, C. D. Y-M. Lin and P. Avouris, *Physics Review B*, 2011, **84**, 205417 1–5.

† In principle, the imaginary conductivity can be calculated from the real part using the Kramers - Kronig relation.

6 T. Otsuji, H. Karasawa, T. Komori, T. Watanabe, M. Suemitsu, A. Satou and V. Ryzhii, *PIERS Proceedings Xian China, March 22-26*, 2010, 756–759.

7 T. Low and P. Avouris, *ACS Nano*, 2014, **75**, 074716 1–7.

8 B. Sandale-rodriguez, R. Yan, S. Rafuque, M. Zhu, W. Li, X. Liang, D. Gundlach, V. Protasenko, M. M. Kelly, D. Jena, L. Liu and H. G. Xing, *Nano Letters*, 2012, **9**, 4518–4512.

9 J. L. Tomaino, A. D. Jameson, J. W. Kevek, M. J. Paul, A. M. van der Znde, R. A. Barton, P. L. McEuen, E. D. Minot, and Y.-S. Lee, *Optical Express*, 2011, **19**, 141–146.

10 J. Maultzsch and C. Thomsen, *Pysical Review B.*, 2004, **70**, 155403.

11 M. Born and E. Wolf, *Principles of Optics: Electromagnetic Theory of Propagation, Interference and Diffraction of Light*, Cambridge University Press, 1993.

12 P. H. Bolivar, M. Brucherseifer, J. G. Rvivas, R. Gonzalo, I. Ederra, A. L. Reynolds, M. Holker and P. Mgt, *IEEE Transaction on Microwave Theory and Techniques*, 2003, **51**, 1062–1066.

13 N. Rouhi, S. Capdevila, D. Jain, K. Zand, W. Y-Y, E. R. Brown, M. L. Jofre and P. Burke, *Nno Res*, 2012, **5**, 667–678.

14 L. A. Falkovsky, *Physics-Uspekhi*, 2008, **51**, 887–897.

15 V. P. Guynin, S. G. Sharapov and J. P. Carbotte, *New Journal of Physics*, 2009, **11**, 095013 1–18.

16 S. Luryi, *Applied Physics Letters*, 1987, **52**, 501–503.